The International Journal of Advanced Manufacturing Technology (2019) 101:1247–1254
https://doi.org/10.1007/s00170-018-3033-3

ORIGINAL ARTICLE

3D laser shock peening as a way to improve geometrical accuracy in selective laser melting

Nikola Kalentics[1] · Andreas Burn[2] · Michael Cloots[3] · Roland E. Logé[1]

Received: 1 October 2018 / Accepted: 12 November 2018 / Published online: 17 November 2018

Abstract

One of the major drawbacks of selective laser melting (SLM) is the accumulation of tensile residual stresses (TRS) in the surface and subsurface zones of produced parts which can lead to cracking, delamination, geometrical distortions, and a decrease in fatigue life. 3D laser shock peening (3D LSP) is a novel hybrid method which introduces a repetitive LSP treatment *during* the manufacturing phase of the SLM process. In this paper, the ability of 3D LSP to convert TRS into beneficial compressive residual stresses and their subsequent effect on the geometrical accuracy of produced parts were investigated. Samples made of Ti6Al4V were manufactured with the 3D LSP process and treated with different processing parameters. Cuboidal samples were used for residual stress measurements, and the evolution of residual stresses was evaluated. Geometrical distortions were measured on bridge-like samples, and the influence on the final sample geometry was quantified. A significant improvement in geometrical accuracy resulting from reduced distortions was observed in all selected 3D LSP processing conditions.

Keywords 3D laser shock peening · Selective laser melting · Laser shock peening · Distortion · Geometrical accuracy · Ti6Al4V

1 Introduction

Selective laser melting (SLM) is one of the most widely researched additive manufacturing (AM) processes in which a part is built in a layer-wise method. SLM is known to be able to produce near net–shape parts with very complex geometries, which are often very difficult or even impossible to manufacture with conventional methods. On the other hand, one of the major drawbacks of the process is the generation of tensile residual stresses (TRS) that accumulate near the surface during the building process and can cause significant distortion in the geometry of the part [1–4]. Accumulation of these stresses can even cause delamination and process failure during the building phase of the part [1, 2, 5]. Different approaches addressing this problem were applied but with limited success. Baseplate preheating was used to decrease the thermal gradients during the building phase of the process, decreasing the TRS accumulation; however, only a limited reduction of up to 40% was observed [6]. Baseplate preheating is usually applied with a maximum temperature of 200 °C since higher chamber temperature will, while having a beneficial effect on the reduction of TRS, inevitably cause lower cooling rates. These reduced cooling rates can lead to undesirable mechanical properties, such as a reduction in yield strength and fatigue limit [7, 8]. Stress relieving by systematic laser rescanning of the previously solidified layer was also applied [6] and showed up to a 55% decrease of TRS. Although somewhat beneficial, laser rescanning of every layer significantly diminishes the productivity of the entire process, which is contrary to the long-lasting tendency of increasing the productivity by applying high power [9, 10] or using multiple lasers [11]. A heat treatment can be applied after the part is made and a reduction of up to 70% in RS can be achieved [6]. All these approaches have shown the ability to decrease TRS, but none of them can introduce beneficial compressive residual stresses (CRS) into the near-surface region of a part, which, if designed accurately, should improve its fatigue life without affecting the geometrical stability [12–14]. Shot peening has been successfully applied as a posttreatment to improve

✉ Nikola Kalentics
nikola.kalentics@epfl.ch

[1] Thermomechanical Metallurgy Laboratory – PX Group Chair, Ecole Polytechnique Fédérale de Lausanne (EPFL), CH-2002 Neuchâtel, Switzerland

[2] Swiss Advanced Manufacturing Center SAMC, Switzerland Innovation Park Biel/Bienne SIPBB, Aarbergstrasse 46, 2503 Biel/Bienne, Switzerland

[3] Irpd AG, Lerchenfeldstrasse 3, 9014 St. Gallen, Switzerland

surface quality, microstructure, and wear resistance and to introduce CRS and increase microhardness of 17–4 stainless steel samples [15, 16]. Although this process can introduce CRS, similarly as for a heat treatment post-process, it cannot address the accumulation of TRS during the building phase which can cause part delamination and process failure.

3D laser shock peening (3D LSP) is a novel AM process patented by the Laboratory of Thermomechanical Metallurgy at EPFL [17]. It is a hybrid process which repeatedly applies laser shock peening (LSP) *during* the building phase of the SLM process, thus giving additional degrees of freedom to adapt and control residual stresses in the part. This approach is applicable to any parts, including those with complex geometry, as long as they can be manufactured by the SLM process.

With the accumulation of tensile residual stresses in large SLM parts, geometrical distortion issues tend to rise. Also, part distortion presents a significant challenge for overhangs and thin-wall structures which are often manufactured by SLM. One approach when dealing with distortions consists in producing parts with an increased volume, with the intention to remove the excess material by machining after the build job. Another approach is the use of more and more sophisticated supports which have a double function as mechanical fixation of the part and as additional heat extraction channels. These compensation strategies need to be taken into account at the design stage [18] and go along with an additional time-consuming pre-processing step and a reduced buy-to-fly ratio. A post-build machining can be time-consuming and altogether reduces the near net–shape advantage of the SLM process. Furthermore, the machining step is limited only to the easily accessible zones of the part and cannot always be applied to the more complex typical SLM geometries involving internal structures.

Geometrical distortion can also cause an elevation in the previously solidified layer, especially while producing overhangs and other thin-walled structures, which can damage the coater during subsequent powder bed deposition. A damaged (scratched) coater is then unable to further deposit an accurate and flat powder bed layer. This leads to defects and porosities in produced parts and usually requires abortion of the part production.

Our previous work has shown that conventional LSP can easily convert TRS into more desirable compressive residual stresses (CRS) [19]. It was also demonstrated that if applied repeatedly in 3D (as in 3D LSP), the process leads to an improved accumulation of CRS [20], both in magnitude and in depth, which is expected to further increase fatigue life compared to conventional LSP-treated parts, or those in the as-built (AB) SLM state.

A recent publication [21] has shown that conventional LSP can be very successful as a posttreatment process of 316L SLM parts both in increasing their fatigue life and reducing geometrical distortions. Due to the material shrinkage during cooling, SLM AB samples exhibit a concave distortion curvature angle on the top surface (an exaggerated image shown in Fig. 1a). In [21], LSP was applied on one side of a 213 mm × 21.6 mm SLM-made 3-mm thick bar, and a convex distortion was observed on the LSP-treated side. With the increase in the number of LSP treatments on the surface, the distortion curvature radius increased and reached 1120 mm after three LSP treatments on the same side (as shown in Fig. 1b). When three LSP treatments were applied on the opposite side, the bar returned to an almost flat state with an arc height of only 250 μm, thus showing the interest of applying LSP as a corrective distortion posttreatment. One drawback of such an approach is that it is limited to thin parts where the effect of LSP as a posttreatment is sufficient to correctively address the SLM distortion. It is also restricted to simple geometries where LSP can reach the external surfaces. Both limitations are of concern when considering SLM parts, which are rarely very thin and simple in shape. Furthermore, residual stresses developed *during* the SLM process can result in shape changes of the part which can inhibit further processing, e.g., elevation of overhangs above the powder coater level. There is, therefore, a strong interest in developing in situ methods for the correction of geometrical distortions which could be applied to *any* SLM part geometry.

In this work, we show for the first time that the 3D LSP strategy can effectively reduce SLM geometrical distortions. Bridge-type Ti6Al4V samples in the AB- and LSP-treated conditions are compared, and contour accuracy is shown to be improved for all considered LSP processing conditions. Compared to previous approaches used to mitigate residual stress-based distortions, this one does not involve any heat treatment since LSP is a cold deformation process. This means that 3D LSP solves the residual stress problem with no detrimental effects on microstructure and mechanical properties.

2 Experimental setup

2.1 SLM parameters and sample geometry

Ti6Al4V was chosen since it is a widely studied SLM material with many applications in aerospace and medical fields [22–24]. The chemical composition is shown in Table 1. Samples were produced in a Concept Laser M2 machine equipped with a fiber laser which was operated in continuous mode. The laser has a wavelength of 1070 nm and a spot size of 150 μm. The SLM processing parameters were determined as follows: laser power of 190 W, scanning speed of 950 mm/s, hatch distance of 0.09 mm, and layer thickness of 0.03 mm. An island scanning strategy was selected such as to minimize TRS and associated geometrical distortion. Oxygen content in the chamber was set below 0.5%. The Ti6Al4V powder was

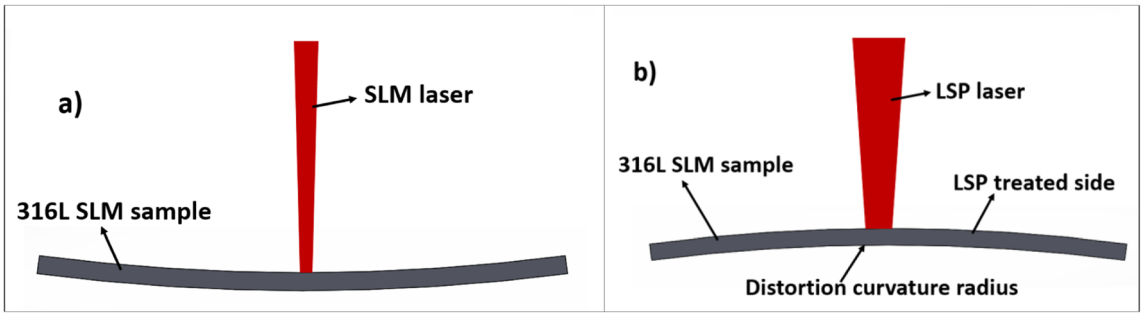

Fig. 1 **a** Exaggerated representation of an AB SLM sample with a concave distortion arc. **b** LSP-treated side of SLM samples with a convex distortion arc of $r = 1120$ mm, modified from [21]

obtained from Concept Laser GmbH, Germany. Its commercial name is CL 41TI ELI.

In the literature, different geometries have been used for evaluating distortion in SLM parts, most notably the cantilever [2], bridge-like [26], and three-prong methods [27]. We have chosen here to produce thinner bridge-like samples in order to increase the number of samples on the baseplate. The sample geometry is shown in Fig. 2a, with dimensions of 25 mm × 10 mm × 5 mm and an arch radius of 2.5 mm. A total of 18 samples were produced, and the minimum thickness of the bridge overhang X (Fig. 2a) was varied between 1, 2, and 3 mm. This gave a total of six samples for each group. While still attached to the baseplate, two samples from each group were treated with a conventional (surface) 2D LSP, two were left in the AB condition, and two were treated with 3D LSP. The two selected 3D LSP conditions considered either $n = 3$ or $n = 10$ SLM layers between two subsequent LSP treatments, respectively.

2.2 Laser shock peening setup

As in [20], the LSP treatment was done on an Nd:YAG SAGA HP class laser from Thales company. For 3D LSP samples, the building phase was paused n layers before the end, and an LSP treatment was applied (see Fig. 3). After the LSP treatment, the final n SLM layers were rebuilt and the LSP process was repeated. In this study, the investigated value of n was {3, 10}. For samples treated by conventional 2D LSP, only a final surface LSP treatment was performed (i.e., LSP was not applied during the SLM building process interruption). All LSP treatments were done while samples were attached to the baseplate. SLM AB samples received no LSP treatment. The LSP process parameters were optimized in our previous work [19, 20] and are considered as best suited for a hybrid 3D LSP machine. It was shown that a lower pulse energy (below 1 J) and a smaller spot size (1 mm) are preferential since such energies can be delivered by a smaller and cheaper laser, which has a higher repetition rate and can be coupled to a fiber beam delivery. These parameters are given in Table 2, and the reader is directed to [20] for more information on the LSP setup.

2.3 Residual stress measurements

Residual stresses measurements were performed on SLM samples made on the same baseplate and with the exact SLM and LSP processing parameters used for the bridge-like distortion samples. The specimen geometry was a 20 × 20 × 5 mm^3 cuboid, and the measurements were made with the hole drilling method (HDM) on a RESTAN-MTS 3000 from SINT Technology in accordance with the ASTM standard E837 [28]. More information on the HDM measurements is provided in [19, 20].

2.4 Distortion measurements

Once sample fabrication and LSP treatments were done, the samples were removed from the baseplate by wire EDM. An alteration of the part geometry by mechanical forces during part removal can, therefore, be excluded. Upon removal, a distortion in their geometry was observed (Fig. 4a, b). Pictures of all samples were taken with a Hirox KH8700 digital microscope. The distortion angle α (Fig. 4b) was measured using SolidWorks 2017 CAD software from Dassault Systemes.

3 Results and discussion

Samples in this study were denoted as the following: "AB" for samples in the SLM as-built condition, "2D LSP" for samples that were treated only with a final LSP treatment on the top surface (as in conventional LSP), and "3D LSP" for samples that were produced as explained in Section 2.2. A further

Table 1 Chemical composition of Ti6Al4V (CL 41TI ELI), wt.% [25]

	Al	V	Fe	C	O	N	H	Ti
Ti6Al4V	5.5–6.5	3.5–4.5	0–0.25	0–0.008	0–0.13	0–0.05	0–0.012	Balance

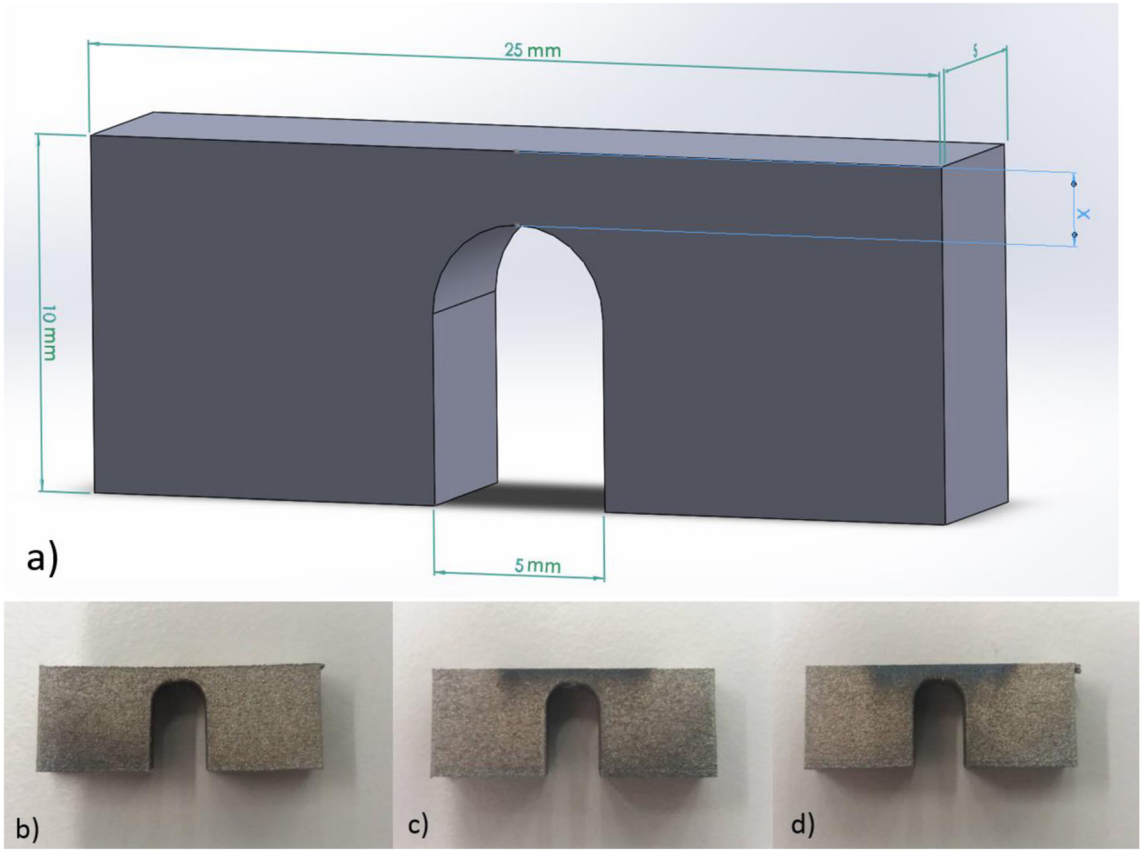

Fig. 2 **a** CAD description of the miniature bridge-like sample. **b** AB sample after detachment from the baseplate. **c** 2D LSP sample. **d** 3D LSP sample

division was done into "3D LSP 3l" and "3D LSP 10l" indicating the value of *n*. In each of these 4 conditions, cuboidal samples for residual stress measurements as well as bridge-like samples with a minimal overhang thickness of 1, 2, and 3 mm for distortion measurements were produced.

3.1 Residual stresses

Residual stresses of Ti6Al4V samples in the AB, 2D LSP, and 3D LSP 3l and 3D LSP 10l conditions are shown in Fig. 5. It can be observed that in the AB SLM state, Ti6Al4V exhibits a tensile RS state with values of up to 422 MPa in the near-surface region and remains tensile throughout the depth of up to 1 mm, which was the measurement limit for the HDM. In all 2D LSP and 3D LSP conditions, TRS are easily converted to CRS with similar values of around − 400 MPa in the subsurface region. The significant difference is that the depth of the compressive stresses, and thus the total volume in the near-surface zone, is increased when LSP is applied in the repetitive 3D LSP mode. In the case of 2D LSP posttreatment, stresses remain compressive up to a depth of 523 μm, while an accumulation of CRS and an increase in their depth (up to 788 and 892 μm) is observed for 3D LSP 3l and 3D LSP 10l samples, respectively. A general trend of an increased depth with the increase in the number of subsequent SLM layers *n* was observed (*n* being here either 3 or 10). This increase in the depth of CRS was

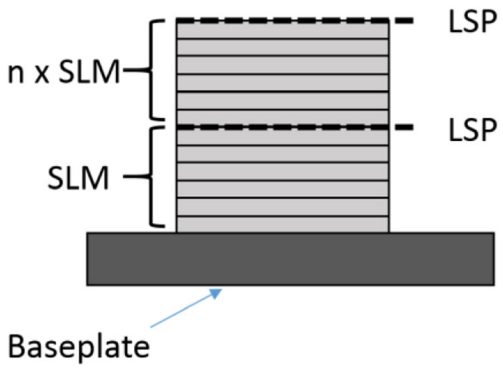

Fig. 3 Schematic of the 3D LSP process with the *n* number of layers between two subsequent LSP treatments

Table 2 LSP process parameters

Wavelength	1064 nm
Pulse duration	6.3 ns
Spot size diameter	1 mm
Pulse energy	0.4 J
Power density	7.2 GW/cm^2
Frequency	5 Hz
Overlap value	80%

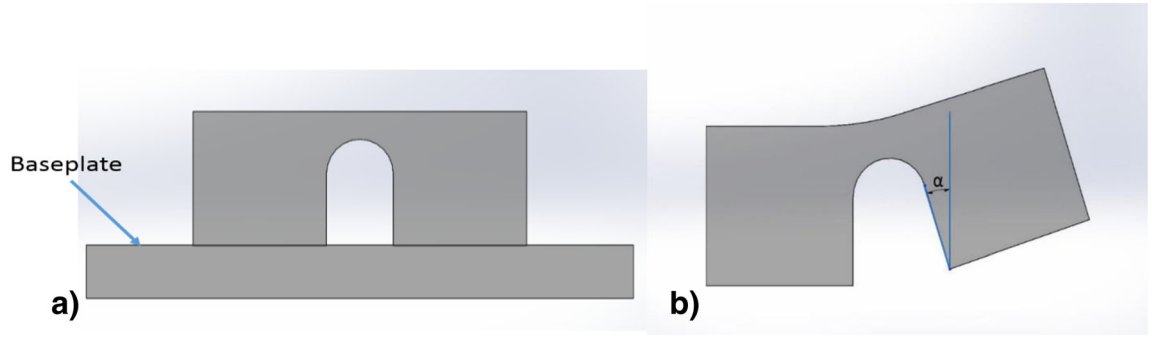

Fig. 4 **a** SLM sample attached to the baseplate before removal. **b** Distorted sample after removal by wire EDM from the baseplate

observed in our previous studies [20] on 316L SLM samples and is here confirmed on a different material. Since melting and solidification during SLM is a very fast process, it introduces only a limited amount of heat, which is insufficient to fully relax the introduced CRS and enable their accumulation. This explains why the following LSP treatment done on top of the rebuilt SLM layers connects well with the previously generated CRS profile, the connection being according to the present results more effective when choosing $n = 10$. It is expected that beyond a critical value n_c, the cumulative effects and the continuity of the CRS will be compromised. The value of n_c itself is assumed to be dependent on the LSP affected depth, processed material, SLM parameters, and scanning strategy and will be further investigated in the future.

3.2 Geometrical distortion

In the case of the AB and 2D LSP condition, for each overhang thickness, two samples were made, and the average value of the distortion angle was taken. The α distortion angle was measured each time; it is reported in Table 3 and plotted in Fig. 6.

3.2.1 As-built state

In the AB SLM state, high TRS accumulate close to the top surface of the part [19, 20, 26, 27]. These stresses create a curl-up distortion angle α [26]. For an overhang of 1 mm thickness, the average value of this angle was measured at 2.21° ± 0.04°. As the overhang thickness increases to 2 mm and 3 mm, the distortion angle slightly decreases to 2.04° ± 0.05° and 1.92° ± 0.03°, respectively. This was expected, as it is well known from the residual stress build-up in welded joints that as the thickness of the welded part is increased, the geometrical distortions are decreasing [29–31].

3.2.2 2D LSP state

After a single LSP surface treatment, it can be observed (Table 3) that the distortion angle is significantly reduced. With the overhang thickness of 1 mm, α is measured as 0.85° ± 0.04°, which represents a 62% improvement compared to the AB state. As the overhang thickness is increased to 2 and 3 mm, α slightly increases to 0.94° ± 0.04° and 0.99° ± 0.02°, respectively. Although conventional 2D LSP can

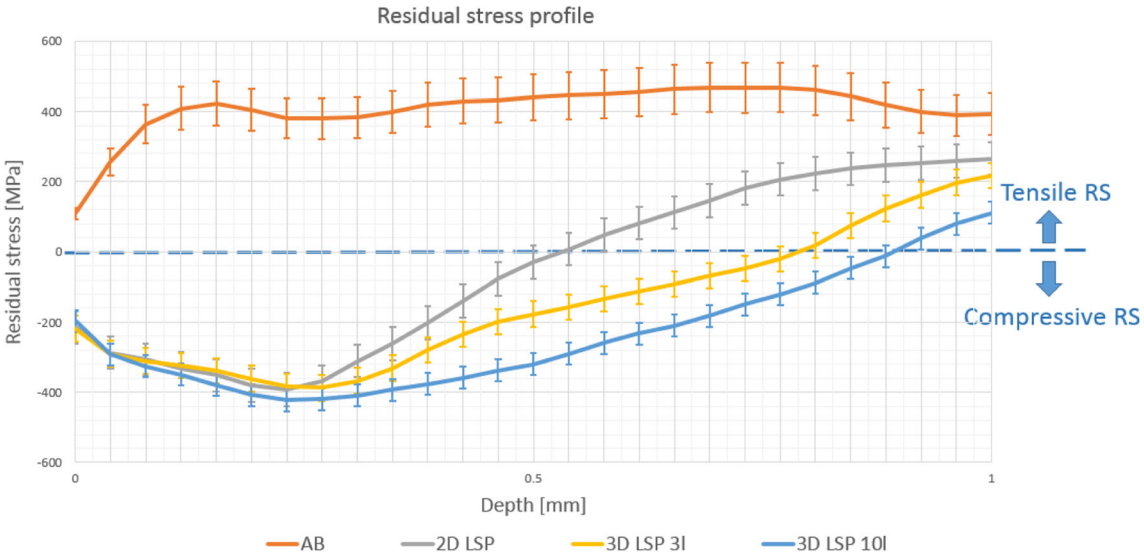

Fig. 5 Residual stress profile of Ti6Al4V samples in the AB, 2D LSP, 3D LSP 3l, and 3D LSP 10l conditions

Table 3 Values of the distortion angle α measured for samples in the AB, 2D LSP, and 3D LSP conditions

Overhang	AB	2D LSP	3D LSP 3 l	3D LSP 10 l
1 mm	2.21° ± 0.04°	0.85° ± 0.04°	0.64°	0.56°
2 mm	2.04° ± 0.05°	0.94° ± 0.04°	0.73°	0.72°
3 mm	1.92° ± 0.03°	0.99° ± 0.02°	0.93°	0.94°

easily convert TRS to compressive RS [19, 20], this effect can be observed only up to a limited affected depth. The introduced CRS are, therefore, not sufficient to fully eliminate the geometrical distortion caused by the accumulated TRS throughout the overhang. With increasing thickness of the overhang, the effect of the LSP becomes comparably smaller, and the improvement on the distortion angle α is reduced.

3.2.3 3D LSP condition

3D LSP samples show a further decrease in the distortion angle α and improvement in the geometrical accuracy compared to conventional 2D LSP and AB conditions. Looking at the 1-mm overhang, α is decreased to 0.64° and 0.56° for 3D LSP 3l and 3D LSP 10l, respectively. These results present an improvement of 69 and 75% compared to the AB state, and 19 and 34% when compared to the conventional 2D LSP condition. This improvement can be correlated to the accumulation of CRS in the subsurface region shown in Section 3.1. The observed increase in depth of CRS with the increase in the number n of SLM layers between two subsequent LSP treatments can explain the slightly better results achieved in the 3D LSP 10l condition.

Values from Table 3 were plotted in Fig. 6 for better clarity. For the AB condition, a clear trend of increase in distortion angle with a decrease in the overhang thickness can be observed, while for the 2D LSP and 3D LSP conditions, a reverse trend appears. 3D LSP leads to improved results in geometrical accuracy compared to conventional 2D LSP treatment. As the overhang thickness increases, the improvement is reduced.

Further improvement for thick geometries is expected with an increase of LSP treatments (> 2). In such cases, a hybrid automated 3D LSP machine - incorporating SLM and LSP processing units - is required to repeatedly apply LSP every n SLM layers and bring the part geometry inside the desired manufacturing tolerances.

4 Conclusions and future work

Residual stresses of SLM Ti6Al4V parts in the AB, 2D LSP posttreatment, and 3D LSP conditions were measured. A geometrical distortion angle α was quantified on bridge-like samples with different overhang thicknesses (1, 2, and 3 mm).

The following conclusion can be drawn:

- In the AB state, Ti6Al4V exhibits TRS up to the measured depth of 1 mm;
- LSP easily converts TRS to CRS, and a cumulative effect on CRS is measured when processing by 3D LSP;
- In the AB state, a significant distortion above 2.2° can be observed, especially pronounced for thinner overhangs;
- With the increase of the overhang thickness, the AB distortion angle slightly decreases;
- With the conventional surface 2D LSP treatment, a decrease in the distortion angle is observed, especially for the thinner overhang;

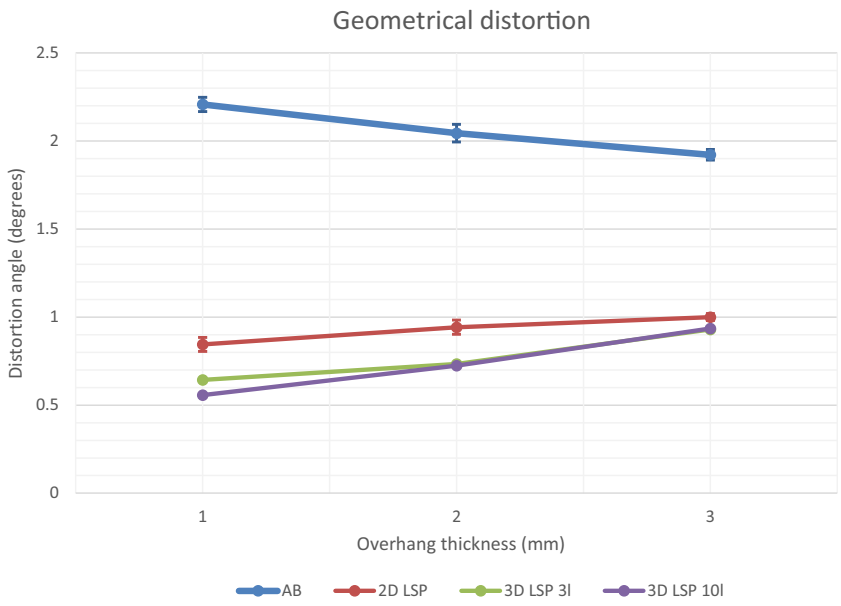

Fig. 6 Values of the distortion angle α measured for samples in the AB, 2D LSP, and 3D LSP conditions for different overhang thicknesses

- 3D LSP shows a clear further improvement in the geometrical accuracy and a decrease in the distortion angle of up to 75% (in the current work) when compared to the AB and 2D LSP conditions;
- For thicker overhangs, an increased number of LSP treatments would need to be applied during SLM processing and would require a hybrid 3D LSP machine.

Further investigations on the influence of 3D LSP on thin overhangs (below 1 mm) will be done. These thinner overhangs are very common in geometries of complex SLM parts, and further optimization of 3D LSP parameters for their treatment is planned.

Acknowledgments The generous support of PX Group to the LMTM laboratory is highly acknowledged.

Funding information This work was financially supported by the CTI project n°25357.2 PFNM-NM.

References

1. Mercelis P, Kruth J-P (2006) Residual stresses in selective laser sintering and selective laser melting. Rapid Prototyp J 12(5):254–265
2. Zaeh MF, Branner G (2010) Investigations on residual stresses and deformations in selective laser melting. Prod Eng 4(1):35–45
3. Li C, Fu CH, Guo YB, Fang FZ (2015) Fast prediction and validation of part distortion in selective laser melting. Procedia Manuf 1:355–365
4. Dunbar AJ, Denlinger ER, Heigel J, Michaleris P, Guerrier P, Martukanitz R, Simpson TW (2016) Development of experimental method for in situ distortion and temperature measurements during the laser powder bed fusion additive manufacturing process. Addit Manuf 12:25–30
5. Kempen K, Vrancken B, Buls S, Thijs L, Van Humbeeck J, Kruth J-P (2014) Selective laser melting of crack-free high density M2 high speed steel parts by baseplate preheating. J Manuf Sci Eng 136(6):061026
6. Shiomi M, Osakada K, Nakamura K, Yamashita T, Abe F (2004) Residual stress within metallic model made by selective laser melting process. CIRP Ann - Manuf Technol 53(1):195–198
7. Rafi HK, Karthik NV, Gong H, Starr TL, Stucker BE (2013) Microstructures and mechanical properties of Ti6Al4V parts fabricated by selective laser melting and electron beam melting. J Mater Eng Perform 22(12):3872–3883
8. Vrancken B, Buls S, Kruth J.-P, and Van Humbeeck J, "Influence of preheating and oxygen content on selective laser melting of Ti6Al4V," in Proceedings of the 16th RAPDASA Conference, 20151101
9. Bremen S, Meiners W, Wissenbach K, Poprawe R (2017) Correlation of the high power SLM process with resulting material properties for IN718. BHM Berg- Hüttenmänn Monatshefte 162(5):179–187
10. Niendorf T, Leuders S, Riemer A, Richard HA, Tröster T, Schwarze D (2013) Highly anisotropic steel processed by selective laser melting. Metall Mater Trans B Process Metall Mater Process Sci 44(4):794–796
11. Masoomi M, Thompson SM, Shamsaei N (2017) Quality part production via multi-laser additive manufacturing. Manuf Lett 13:15–20
12. Zhang XC, Zhang YK, Lu JZ, Xuan FZ, Wang ZD, Tu ST (2010) Improvement of fatigue life of Ti–6Al–4V alloy by laser shock peening. Mater Sci Eng A 527(15):3411–3415
13. Dorman M, Toparli MB, Smyth N, Cini A, Fitzpatrick ME, Irving PE (2012) Effect of laser shock peening on residual stress and fatigue life of clad 2024 aluminium sheet containing scribe defects. Mater Sci Eng A 548:142–151
14. Charles TW, Montross S (2002) Laser shock processing and its effects on microstructure and properties of metal alloys: a review. Int J Fatigue 24(10):1021–1036
15. AlMangour B, Yang J-M (2016) Improving the surface quality and mechanical properties by shot-peening of 17-4 stainless steel fabricated by additive manufacturing. Mater Des 110:914–924
16. AlMangour B, Yang J-M (2017) Integration of heat treatment with shot peening of 17-4 stainless steel fabricated by direct metal laser sintering. JOM 69(11):2309–2313
17. Kalentics N, Logé R, and Boillat E (2017) "Method and device for implementing laser shock peening or warm laser shock peening during selective laser melting," US20170087670 A1
18. Afazov S, Denmark WAD, Lazaro Toralles B, Holloway A, Yaghi A (2017) Distortion prediction and compensation in selective laser melting. Addit Manuf 17:15–22
19. Kalentics N, Boillat E, Peyre P, Ćirić-Kostić S, Bogojević N, Logé RE (2017) Tailoring residual stress profile of selective laser melted parts by laser shock peening. Addit Manuf 16:90–97
20. Kalentics N, Boillat E, Peyre P, Gorny C, Kenel C, Leinenbach C, Jhabvala J, Logé RE (2017) 3D laser shock peening – a new method for the 3D control of residual stresses in selective laser melting. Mater Des 130:350–356
21. Hackel L, Rankin JR, Rubenchik A, King WE, and Matthews M (2018) "Laser peening: a tool for additive manufacturing post-processing," Addit Manuf
22. Yadroitsev I, Krakhmalev P, Yadroitsava I (Jan. 2014) Selective laser melting of Ti6Al4V alloy for biomedical applications: temperature monitoring and microstructural evolution. J Alloys Compd 583:404–409
23. A. A. Antonysamy (2012) "Microstructure, texture and mechanical property evolution during additive manufacturing of Ti6Al4V alloy for aerospace applications," [Thesis]. Manchester, UK: The University of Manchester; 2012, [Online]. Available: https://www.escholar.manchester.ac.uk/uk-ac-man-scw:160535. [Accessed: 12-Apr-2018]
24. Campanelli SL, Contuzzi N, Ludovico AD, Caiazzo F, Cardaropoli F, Sergi V (2014) Manufacturing and characterization of Ti6Al4V lattice components manufactured by selective laser melting. Materials 7(6):4803–4822
25. (2018)"1709 CL 41TI ELI_layer.indd - Datasheet_CL_41TI_ELI.pdf." [Online]. Available: https://www.concept-laser.de/fileadmin//user_upload/Datasheet_CL_41TI_ELI.pdf. [Accessed: 12-Apr-]
26. Kruth J-P, Badrossamay M, Yasa E, Deckers J, Thijs L, and Van Humbeeck J (2010) "Part and material properties in selective laser melting of metals," presented at the Proceedings of the 16th International Symposium on Electromachining
27. Sillars SA, Sutcliffe CJ, Philo AM, Brown SGR, Sienz J, Lavery NP (2018) The three-prong method: a novel assessment of residual stress in laser powder bed fusion. Virtual Phys Prototyp 13(1):20–25
28. Casavola C, Campanelli SL, Pappalettere C Experimental analysis of residual stresses in the selective laser melting process. In: Proccedings of the XIth International Congress and Exposition, Orlando. Florida, USA, p 2008

29. Renzi C, Panari D, and Leali F (2018) "Predicting tolerance on the welding distortion in a thin aluminum welded T-joint," Int J Adv Manuf Technol, pp. 1–16
30. Mahapatra MM, Datta GL, Pradhan B, Mandal NR (2006) Three-dimensional finite element analysis to predict the effects of SAW process parameters on temperature distribution and angular distortions in single-pass butt joints with top and bottom reinforcements. Int J Press Vessel Pip 83(10):721–729
31. Deng D, Liang W, Murakawa H (2007) Determination of welding deformation in fillet-welded joint by means of numerical simulation and comparison with experimental measurements. J Mater Process Technol 183(2):219–225